Green Energy and Technology

Ali M. Eltamaly
Almoataz Y. Abdelaziz
Ahmed G. Abo-Khalil *Editors*

Control and Operation of Grid-Connected Wind Energy Systems

Springer

Green Energy and Technology

Climate change, environmental impact and the limited natural resources urge scientific research and novel technical solutions. The monograph series Green Energy and Technology serves as a publishing platform for scientific and technological approaches to "green"—i.e. environmentally friendly and sustainable—technologies. While a focus lies on energy and power supply, it also covers "green" solutions in industrial engineering and engineering design. Green Energy and Technology addresses researchers, advanced students, technical consultants as well as decision makers in industries and politics. Hence, the level of presentation spans from instructional to highly technical.

Indexed in Scopus.

More information about this series at http://www.springer.com/series/8059

Ali M. Eltamaly · Almoataz Y. Abdelaziz ·
Ahmed G. Abo-Khalil
Editors

Control and Operation of Grid-Connected Wind Energy Systems

Springer

Editors
Ali M. Eltamaly
Sustainable Energy Technology Center
King Saud University
Riyadh, Saudi Arabia

Almoataz Y. Abdelaziz
Electrical Power and Machines Department
Ain Shams University
Cairo, Egypt

Ahmed G. Abo-Khalil
Electrical Engineering Department
Majmaah University
Almajmaah, Saudi Arabia

ISSN 1865-3529 ISSN 1865-3537 (electronic)
Green Energy and Technology
ISBN 978-3-030-64335-5 ISBN 978-3-030-64336-2 (eBook)
https://doi.org/10.1007/978-3-030-64336-2

This Springer imprint is published by the registered company Springer Nature Switzerland AG
The registered company address is: Gewerbestrasse 11, 6330 Cham, Switzerland

Preface

Renewable energy systems are becoming more attractive for generating electric power due to their sustainability, environmental friendliness, can be used as a replacement for the dependency on fossil fuels, and they can be localized near the loads to add support to the electric power system. Wind energy is one of the fastest growing renewable energy systems and with the increasing improvements to the control system of wind energy systems, it can increase its penetration to the electric power system mix. The generated energy and the stability of the wind energy systems depend mainly on the wind speed variation and the improvement in the control system of this energy source will help to increase their use for generating electric energy. This book is introduced to present the control and operations of the integration of wind energy systems with electric power systems. The book introduced the size of the excitation capacitor required when using a three-phase induction generator with an accurate model for the losses in the rotor and stator of the self-excited induction generator. Also, the use of a Double-fed Induction Generator (DFIG) as a generator in wind energy applications is getting more attention in many chapters of this book. The control of generated power in the DFIG and maximum power tracking is introduced and discussed in many chapters of this book. The power quality and harmonics injected into the power system are introduced and discussed. Many techniques to overcome (treat) the effects of harmonics on the power system due to the integration of renewable energy systems to the electric utility are introduced and discussed. The communication techniques used in the control and operation of the wind energy system and the SCADA systems are introduced to show how they can control the wind energy systems. Many chapters have been introduced in the book to show the effect on the power system when the wind energy system is used as a distributed generation source. Also, smart optimization techniques have been used in one chapter for performance and control improvement and the maximum power point tracking of the wind energy system. Moreover, planning, design, and cost analysis of the wind energy system and economic analysis of the wind energy system are introduced in many chapters and how they can be used in a hybrid system with other renewable energy sources is introduced and discussed. The selection of wind turbine suitable for sites and the criteria used to choose the best sites are introduced in detail.

This book is introducing a good overview on how to use the wind energy system working standalone and integrated with the electric utility. These subjects introduced in this book will help students, researchers, designers, and decision-makers for a better understanding of the operation and control of wind energy systems and how it can be interconnected with an electric utility and the financial details of installing wind energy systems. Moreover, this book will be very interesting for the readers who are looking for using wind energy systems to feed loads in isolated areas as well as on the utility scale. It will also help them to know the wind energy systems' characteristics, modeling, operation, challenges, maximum power tracking, and practical implementation.

Riyadh, Saudi Arabia — Ali M. Eltamaly
Cairo, Egypt — Almoataz Y. Abdelaziz
Almajmaah, Saudi Arabia — Ahmed G. Abo-Khalil

Acknowledgment

The editors of this book would like to thank the authors and reviewers for their contributions and efforts. Moreover, we would like to thank all colleagues from K. A. CARE Energy Research and Innovation Center, Riyadh, Saudi Arabia for their help and efforts.

Contents

About the Editors

Ali M. Eltamaly (Ph.D.–2000) is a Full Professor at Mansoura University, Egypt, and King Saud University, Saudi Arabia. He received B.Sc. and M.Sc. in Electrical Engineering from Al-Minia University, Egypt in 1992 and 1996, respectively. He received Ph.D. in Electrical Engineering from Texas A&M University in 2000. His current research interests include renewable energy, smart grid, power electronics, motor drives, power quality, artificial intelligence, evolutionary and heuristic optimization techniques, and distributed generation. He has published 20 books and book chapters and he has authored or coauthored more than 200 refereed journals and conference papers. He has published several patents in the USA patent office. He has supervised several M.S. and Ph.D. theses worked on several National/International technical projects. He got Distinguished Professor award for Scientific Excellence, Egyptian supreme council of Universities, Egypt, June 2017, and he has awarded many prizes in different universities in Egypt and Saudi Arabia. He is participating as an editor and associate editors in many international journals and chaired many international conferences' sessions. He is Chair Professor of Saudi Electricity Company Chair in power system reliability and security, King Saud University, Riyadh, Saudi Arabia.

Almoataz Y. Abdelaziz (SMIEEE' 2015) He received B.Sc. and M.Sc. in Electrical Engineering from Ain Shams University, Cairo, Egypt, in 1985 and 1990, respectively, and Ph.D. in Electrical Engineering according to the channel system between Ain Shams University, Egypt, and Brunel University, U.K., in 1996.

He is currently a Professor of Electrical Power Engineering at Ain Shams University. He has authored or coauthored more than 350 refereed journals and conference papers and 20 book chapters. He has supervised more than 70 M. Sc. and 15 Ph.D. theses in his research areas, which include the applications of artificial intelligence, evolutionary and heuristic optimization techniques to power systems power system operation, planning, and control.

Dr. Abdelaziz is the Chairman of IEEE Education Society chapter in Egypt, a Senior Editor of Ain Shams Engineering Journal, Editor of Electric Power Components & Systems Journal, Editorial Board member, Editor, Associate Editor, and Editorial Advisory Board member for many international journals.

He is also a senior member in IEEE, a member in IET, and the Egyptian Sub-Committees of IEC and CIGRE'. He has been awarded many prizes for distinct researches and for international publishing from Ain Shams University, Egypt.

Ahmed G. Abo-Khalil received the Bachelor and Master of Science in Engineering from Assiut University, Egypt, and Ph.D. from the School of Electrical and Computer Engineering, Yeungnam University, South Korea, in 2007. In 2008, he joined Rensselaer Polytechnic Institute, NY, USA, as a postdoc researcher and worked on a renewable energy project. From 2009 to 2010, he was a Postdoctoral Research Fellow in the Korean Institute of Energy Research, Daejeon, South Korea, working on photovoltaic power conversion systems. In 2010, he moved to Assiut University, Egypt, as an Assistant Professor. He works now as an Associate Professor with the Department of Electrical Engineering, Majmaah University, Almajmaah, Kingdom of Saudi Arabia.

Modeling and Effect of Core Loss in AC Three-Phase Self-excited Generators Used in Wind Energy Applications

Saleh Al-Senaidi, Abdulrahman Alolah, and Majeed Alkanhal

Abstract Green renewable energy sources have been introduced as alternatives to avoid the environmental impact of the hazardous waste of conventional power generation. One of these remarkable exploited green sources is wind energy. Self-Excited AC Generators, namely, three-phase Self-Excited Induction (SEIG) and Reluctance (SERG), generators are used to convert wind power to electric power. Extensive research studies have been carried out on the analyses of dynamic, transient, as well as steady-state performance of these generators. In most of these studies, core losses were neglected. However, different methods have been attempted to consider the core loss by adding resistance to the model of the generators. The values of this resistance are taken as either; (i) fixed, (ii) linearly proportional to the magnetizing reactances (X_m or X_d), or (iii) variable as a polynomial function of X_m (or X_d). This chapter presents a comparative study to assess the above-mentioned three methods under different operating conditions of (SEIG) and (SERG) generators. The effect of neglecting the core loss on the analysis are studied. The method no. (iii) above is used as a reference to evaluate the errors in the other methods. The generator performance resulted from the three methods is shown and compared. Experimental verifications are included to illustrate the most accurate method to account for core loss in generator analysis.

Keywords Core loss · Self-excited · Reluctance generator · Induction generator · Three phase · Steady state · Wind energy

S. Al-Senaidi (✉) · A. Alolah · M. Alkanhal
Department of Electrical Engineering, College of Engineering, King Saud University, Riyadh, Saudi Arabia
e-mail: salih@ksu.edu.sa

A. Alolah
e-mail: alolah@ksu.edu.sa

M. Alkanhal
e-mail: majeed@ksu.edu.sa

A. M. Eltamaly et al. (eds.), *Control and Operation of Grid-Connected Wind Energy Systems*, Green Energy and Technology,
https://doi.org/10.1007/978-3-030-64336-2_1

List of Symbols

a	P.u. speed.
C, X_c	Value of excitation capacitance (μF) and its p.u. reactance at base frequency, respectively.
$C_{\min}$	Minimum excitation capacitance (μF).
V_o	P.u. terminal voltage.
E_q, E_d	P.u. quadrature and direct magnetizing voltages, respectively.
F, u	P.u. frequency and speed, respectively.
I_q, I_d	P.u. quadrature and direct magnetizing currents, respectively.
I_s, I_c, I_L, I_e	P.u. stator, excitation capacitance, load, and core loss currents, respectively.
R_s, R_r, R_e, R_L	P.u. stator, rotor, core loss, and load resistances, respectively.
E_R, E_g	P.u. air gap voltages of SERG and SEIG, respectively.
X_d	P.u. direct axis saturated magnetizing reactance.
X_o, X_m	P.u. unsaturated and saturated magnetizing reactances at base frequency, respectively.
X_q	P.u. quadrature axis magnetizing reactance at base frequency.
X_L, X_r, X_s	P.u. load, and rotor and stator leakage reactances at base frequency, respectively

1 Introduction

The induction and synchronous reluctance machines are considered self-excited when the appropriate value of capacitors are attached to their terminals while the rotors are driven at suitable speeds. The analyses of the dynamic, transient, and steady state of self-excited AC generators have been covered deeply in the literature albeit the core losses have been largely ignored in the studies. In this chapter, the core losses are modeled in a more accurate function, which is associated with the degree of saturation. This association is obtained experimentally and integrated as a nonlinear model of the SERG and SEIG. The performance of the system is obtained by using an optimization technique to solve the nonlinear models. The result is a novel group of curves that accurately describe the performance of the generator when core losses are taken into consideration. Experimental and computed curves match so much that show the accuracy of the presented models.

In SEIG, some publications completely left out the core loss effects [1–10] while others simply used the motor model of the core loss or assumed a constant resistance in shunt with the magnetizing reactance as a replacement for the core loss [11–17]. These approaches are adequate for motor operation because motors operate near the unsaturated region. On the other hand, SEIG operates in the saturated region [1–5] which is largely affected by variations in load, shaft speed, the value of excitation

capacitor, and load's power factor. The changes in the level of saturation change the core loss and hence the operating parameters of the generator.

The main advantages of SERG over SEIG are constant frequency operation as well as lower copper and core losses [18–25]. An equivalent circuit similar to a SEIG is presented in [24] to simplify the analysis of a SERG; however, the effect of an essential parameter of the reluctance machine, which is the saliency ratio, was ignored in the analysis [26]. A model was developed for SERG in [23, 25] by applying Park's d-q transformation with consideration of the effect of magnetic saturation and saliency on the performance analysis. Further development of this analysis with variable speed is made in [27, 28] to predict capacitance requirements and operating limits. However, the above studies do not include core losses of the generator in the analyses. An interesting method for analyzing the SERG has been presented in [29] by considering both core losses and saliency. This method is not appropriate for situations where capacitors are connected to the terminals of the generator for self-excitation as the excitation is generated by connecting a rectifier bridge and a DC supply. The analysis in [30] was performed by modifying that in [24], and the core loss and saliency were considered. However, in this analysis, the core loss was assumed to be constant and represented by a constant resistance irrespective of the saturation effects; furthermore, the analysis was valid only for a fixed speed.

On the other hand, good analysis in [31] was developed for the SERG and was verified experimentally by considering the core loss as a variable resistance. The value of the resistance is considered to be directly proportional to the magnetizing reactance, i.e., $R_e = k\, X_d$, where k is a proportionality constant.

As a matter of fact, any variation or change in the operation conditions, such as the load power factor, load impedance (R_L and/or X_L), speed, and/or excitation capacitance, will definitely vary the level of saturation of the SERG. The saturation-level variation will change the saturated magnetizing reactance, X_d, core loss, and the air gap voltage, and hence the performance of the SERG. For this reason, the core loss needs to be linked to the level of saturation in the SERG by modeling it as a variable parameter.

The aim of this chapter is to propose an accurate model of the core loss that takes into consideration any change in the level of saturation due to changes in speed (u), excitation capacitance (C), load (Z_L), and its power factor (pf) as mention earlier. To achieve this, the core loss resistance is modeled as a variable that is influenced by the level of saturation in the generator. The benefit of this model is that it can be included in the future design of SEIG and SERG to take into consideration the high and varying saturation levels in the generators. In the following sections, the core loss is linked to the level of saturation by modeling it mathematically as a variable function of saturation level that increases the accuracy of the analysis of SEIG and SERG. The accuracy of the proposed core loss model is confirmed by a set of experimental tests that agree with the simulated results.

2 Three-Phase Self-excited Induction Generator

The SEIG is mostly used in isolated power supply and the mode of excitation is achieved by connecting some predetermined optimal value of capacitor bank across the stator terminals. The capacitor banks supply the required reactive power by the induction generator and accordingly corrects the power factor of the machine. Using only the permanent magnetism of the machine, the capacitor bank resonates with the inductance of the machine to build up the voltage of the IG terminals from near to zero to the desired level. Figure 1 illustrates the scheme of the SEIG.

2.1 Analysis

The equivalent circuit in a per phase of a three-phase SEIG with *R-L* load is shown in Fig. 2. Saturation effects are taken into consideration by modeling the core loss resistance R_c, and the magnetizing reactance X_m as variable parameters. The basic parameters of the generator are obtained from the usual DC, locked rotor, and no-load running at synchronous speed tests. From the DC and the locked rotor tests, the values of R_s, R_r, X_s, and X_r are determined. The magnetization curve of the generator was obtained using a no-load running test while the rotor was driven at synchronous speed. This curve reveals the variation of R_c and X_m against the air-gap voltage (or magnetizing current) as shown in Fig. 3. This figure shows that X_m and R_c are varying in relation to the level of saturation in accordance with the air-gap voltage. Figure 4a

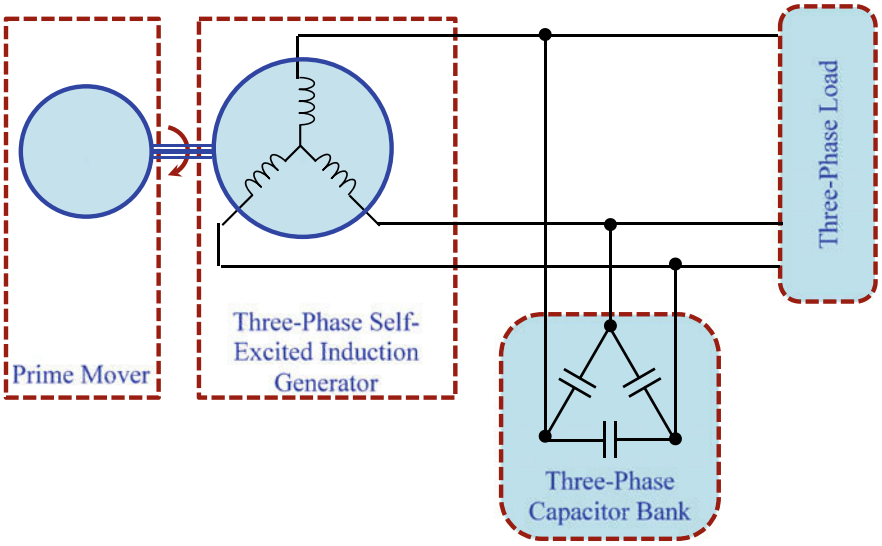

Fig. 1 Three-phase self-excited induction generator

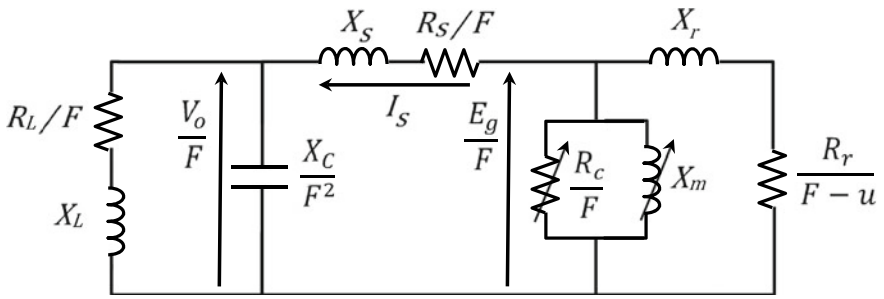

Fig. 2 SEIG per-phase equivalent circuit under the proposed core loss model

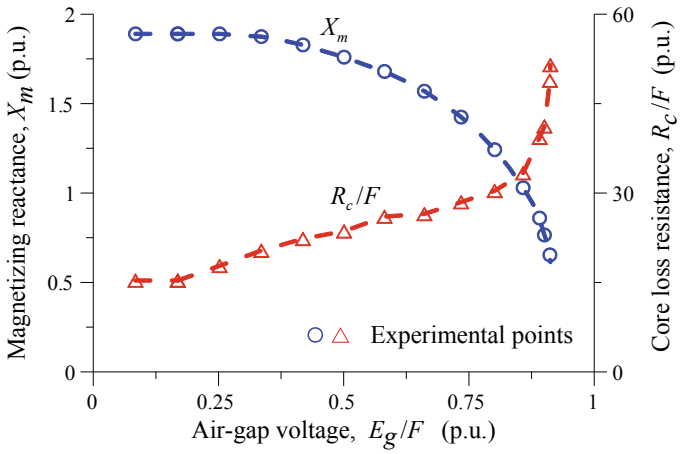

Fig. 3 Variation in R_c/F and X_m against E_g/F in the generator under study

shows a redevelopment of the magnetizing curve shown in Fig. 3 that is essential to obtain the SEIG performance. X_m and R_c are varying because they are considered as variable parameters since they are linked to the saturation level in the generator which varies according to the operating conditions. This fact, to the best knowledge of the authors, is ignored in all the literature of SEIGs [1–9].

2.1.1 Core Loss Modeling

The research gap in the literature as mentioned above is filled by modeling the rate change of the core loss, R_c, with the magnetizing reactance, X_m, as illustrated in Fig. 4b. Experimental results of Fig. 4b shows that the core loss, R_c, varies largely with X_m and can be described mathematically with a fourth-degree polynomial fitted curve. From this model, any change in u, Z_L, and C that leads to the change in the level of saturation can be captured in the change of X_m and consequently in the value

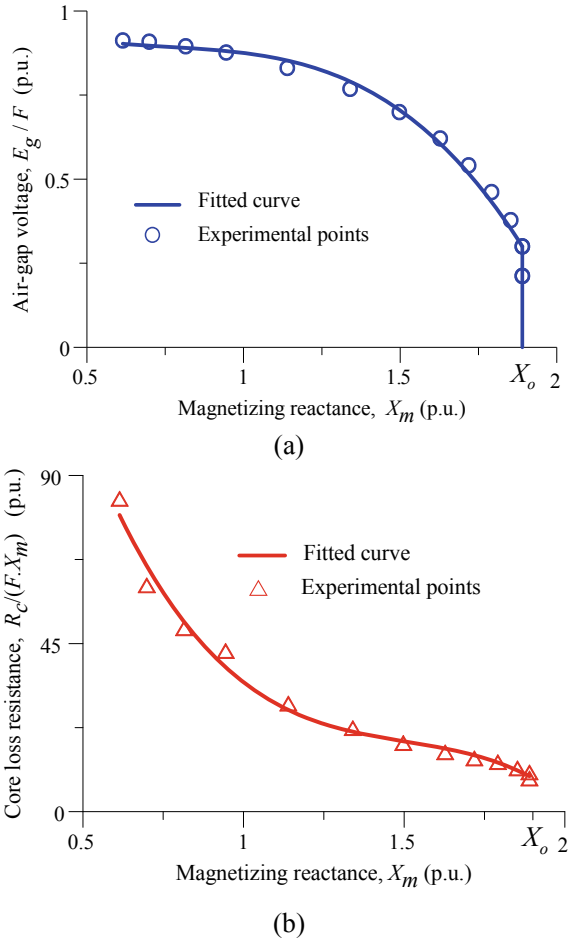

Fig. 4 Variation in E_g/F and $R_c/(F\,X_m)$ against X_m: **a** E_g/F, **b** $R_c/(F\,X_m)$

of R_c. The curve of the air-gap voltage (E_g) against X_m in Fig. 4a is expressed for computational purposes by a set of piecewise linear functions [1, 32] or by making use of curve fitting with an appropriate degree of a polynomial function as developed by the authors earlier [3].

With the same concept, the variation of the core loss against X_m is also fitted in the same manner as another polynomial function, as shown in Fig. 4b. The fitted curves are expressed as

$$E_g/F = \sum_{i=0}^{n} k_i X_m^i \tag{1}$$

$$R_c/(F \cdot X_m) = \sum_{i=0}^{r} m_i X_m^i \tag{2}$$

where m_i and k_i are the coefficients of the polynomials.

The polynomial coefficients are determined experimentally and are given in the Appendix. This method does not alter the characterization given in [1], because the variation in R_c is linked to the variation in X_m (R_c is a function of X_m (i.e., $R_c = f(X_m)$).

2.1.2 Loop-Impedance Solution

In the circuit of Fig. 2, the total impedance, Z_t, across R_c and X_m branch is expressed as

$$Z_t = ((Z_s + (Z_L//Z_C))//Z_r) + Z_m \tag{3}$$

where $Z_s = R_s/F + jX_s$, $Z_L = R_L/F + jX_L$, $Z_r = R_r/(F-u) + jX_r$, $Z_m = (R_c/F)//(jX_m)$, and $Z_c = -jX_c/F^2$.

When the system in Fig. 2 operates at the steady-state condition, the voltage across Z_t is equal to zero [5], i.e.,

$$I_s Z_t = 0 \tag{4}$$

In steady state, there is a passing current in the stator windings (i.e., $I_s \neq 0$), which implies that $Z_t = 0$. From this, the two equations can be expressed as

$$Re(Z_t) = 0 \tag{5}$$

$$Im(Z_t) = 0 \tag{6}$$

Equations (5) and (6) can be solved for two unknowns such as (X_m and F), (X_c and F), (u and F), or (Z_L and F).

Solving the nonlinear equations of (5) and (6) can be done using many schemes that are reported in the literature. A scheme that was presented in [11] used the Newton–Raphson method to solve for the unknowns. Another scheme was given in [1, 2] by rearranging the two equations as two polynomials of high degree in the desired unknown along with the frequency, F. Nevertheless, these schemes cannot fit the proposed model given in this section because the core loss is assumed to be varying. Instead, solving Eqs. (5) and (6) under a variable core loss can be obtained by applying optimization-based schemes, such as the one presented in [3] as described below.

2.1.3 Method of Solution

An optimization-based program was built to solve Eqs. (5) and (6) for the desired unknowns. The desired unknowns can be F and X_m, X_c, Z_L, or u that are obtained by minimizing the value of Z_t (i.e., $|Z_t| = 0$). The system performance of Fig. 2 can be obtained once the unknowns are found with the help of the magnetization curve.

The flowchart of the optimization-based program that solves for X_m and F against the speed is shown in Fig. 5. For obtaining other unknowns such as (F and u), (F and

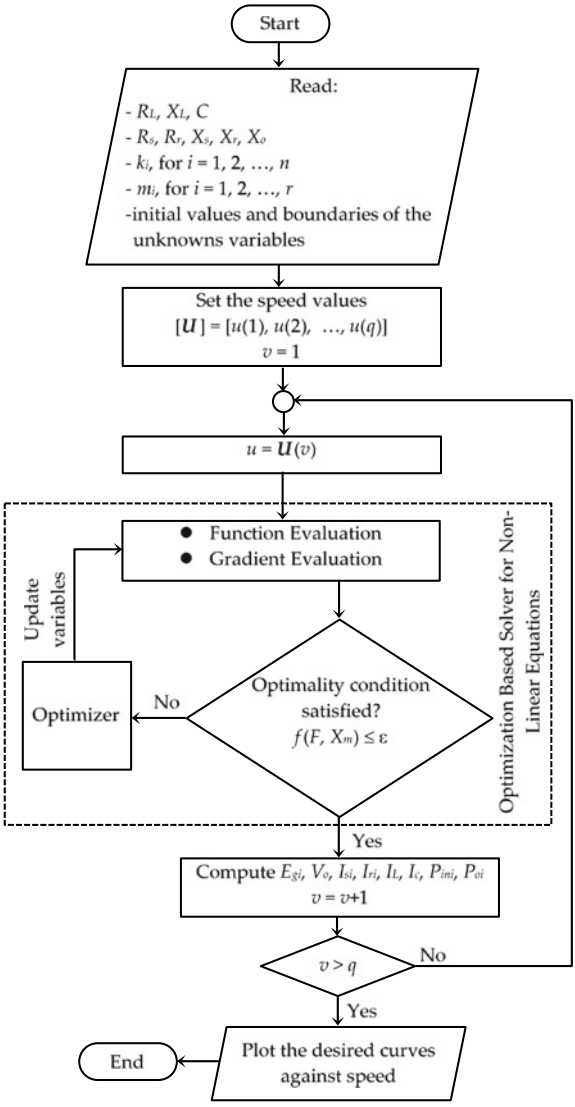

Fig. 5 Optimization program flowchart to obtain the performance of the SEIG against the speed ($\varepsilon = 1 \times 10^{-5}$)

Z_L), and (F and X_c), similar programs were developed. This scheme is built with the MATLAB functions "constr" and "fmincon", which are classical enhanced numerical gradient-type optimizers. This gradient-based optimization scheme is applied to solve the developed model due to its efficiency and reliability in handling nonlinear problems. The process is iterative with the basic steps shown in the flowchart of Fig. 5. The optimization is initialized at a randomly chosen feasible starting point in order to enhance the chance of the algorithm to converge to global minima. The optimization algorithm makes use of both the model evaluation as well as the directed gradient to converge toward the optimal point [33, 34]. The error tolerance, ε, was set to be 1×10^{-5}.

2.2 Results and Discussion

The value of F, R_c, X_m, as well as other parameters of the system shown in the circuit of Fig. 2 vary with any variation in the controlled parameters (u, Z_L, and C). Under different load conditions, Fig. 6 presents the variations in X_m, R_c, V_o, and I_s, against C. The curve value of X_m drops to a minimum as C is being increased and then starts growing up as shown in Fig. 6a. On the other hand, the curve value of R_c decreases and increases irrespective of the value of X_m. Figure 6b shows that the stator current, I_s, increases as the excitation capacitance increases then it decreases against any increase in C. A similar observation is noticed for the terminal voltage, V_o in the same figure. It is worth mentioning that the machine operates as a generator when X_m is less than X_o (i.e., $X_m \leq X_o$) [1–4].

The variations in frequency, F, and minimum excitation capacitor ($C_{\min}$) against the power factor (pf) at two different loads are shown in Fig. 7. This case was obtained by keeping the speed constant at 1.0 p.u. and X_m was assumed to have a value equal to X_o. The value of $C_{\min}$ is higher at the lower value of Z_L and vice versa. Opposite observation is noticed for F. In addition, as the power factor increases from zero to one, the frequency decreases in a small amount while the value of $C_{\min}$ increases in a small amount then decreases at a noticeable rate. When the capacitor and speed are fixed at 40 μF and 1.0 p.u., respectively, the variation in X_m and F versus power factor is shown in Fig. 8. It is noticeable that the larger the value of Z_L, the lower the value of X_m. Again, the frequency decreases in a small amount as the power factor increases from zero to one. The decrement is more for the minimum load impedance, Z_L. For the same value of the capacitor and speed of Fig. 8, the variation in the stator current and terminal voltage against the power factor is shown in Fig. 9. At a higher value of load impedance, the terminal voltage is approximately constant at a lower value of X_m as shown in Fig. 8.

The variation in R_c and X_m against u is shown in Fig. 10a for two different loads while C is kept fixed at 30 μF. For the same case, Fig. 10b shows the variation in the stator current and the terminal voltage versus speed. This figure shows clearly that R_c changes as the speed varies to agree to the measured results shown in Fig. 3.

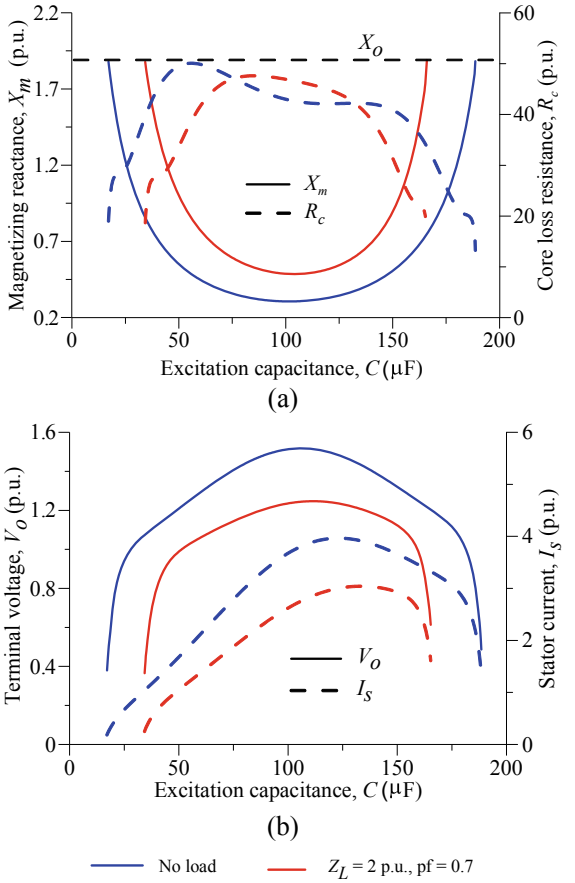

Fig. 6 Variation against C for two different loads ($u =$ 1.0 p.u.): **a** Core loss resistance R_c and magnetizing reactance X_m, **b** stator current I_s and terminal voltage V_o

2.3 Experimental Verification

2.3.1 Setup

Under different conditions, experimental tests were carried out on the machine studied above to verify the proposed model. Figure 11 shows the experimental setup to obtain the performance of the machine under study. A DC motor that is controlled by a variable DC power supply drives the SEIG rotor. The excitation of the generator is achieved by using a star connected capacitor bank. The measurements of the mechanical and electrical quantities such as power, power factor, current, voltage, speed, and frequency were made by a computerized measurement unit (model CEM-U/Elettronica Veneta).

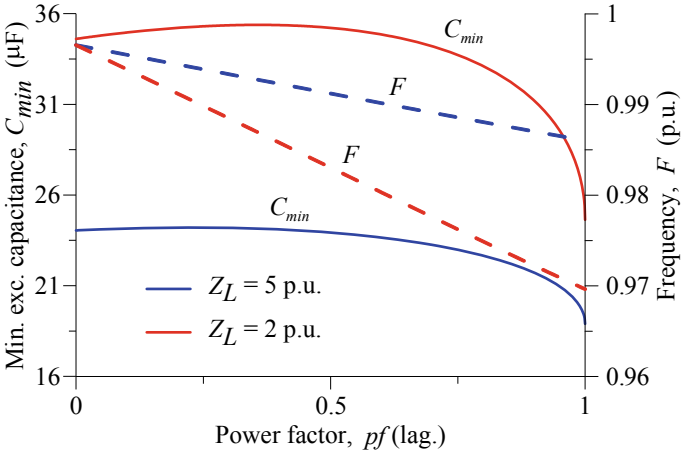

Fig. 7 Variation in frequency F and minimum excitation capacitance $C_{\min}$ against power factor pf for two different loads ($u = 1.0$ p.u.)

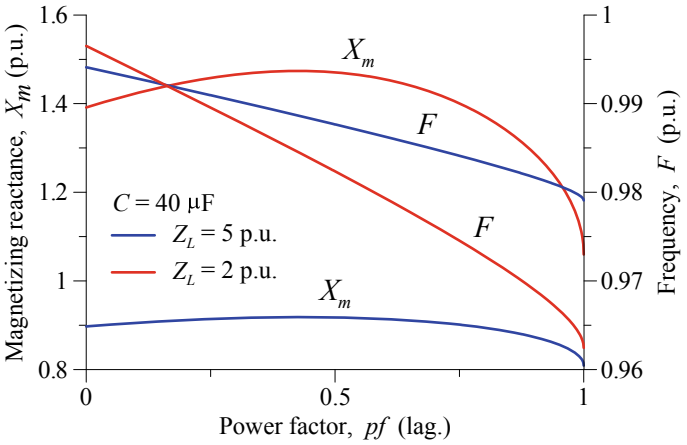

Fig. 8 Variation in frequency F and magnetizing reactance X_m against power factor pf for two different loads ($u = 1.0$ p.u.)

2.3.2 Performance Measurements

The variation in the stator current, I_s, and terminal voltage, V_o, versus C at a fixed speed ($u = 1.0$ p.u.) is shown in Fig. 12. The variation in I_s and V_o versus speed at a fixed capacitor ($C = 30$ μF) is shown in Fig. 13. Under different excitation capacitor values, Fig. 14 shows the system performance similar to that of Fig. 13. As expected, these figures show that an increase in speed or C will result in an increase in I_s and V_o. In addition, the frequency increases as u increases. These figures show

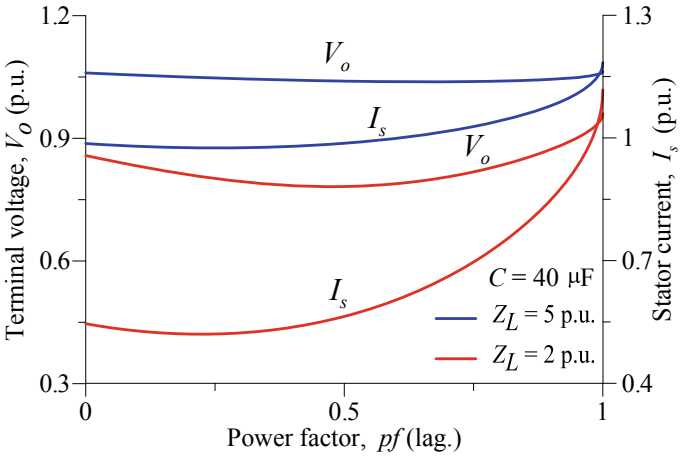

Fig. 9 Stator current I_s and Terminal voltage V_o against power factor pf for two different loads ($u = 1.0$ p.u.)

Fig. 10 Variation against speed for two different load conditions ($C = 30$ μF): **a** Core loss resistance R_c and magnetizing reactance X_m, **b** stator current I_s and terminal voltage V_o

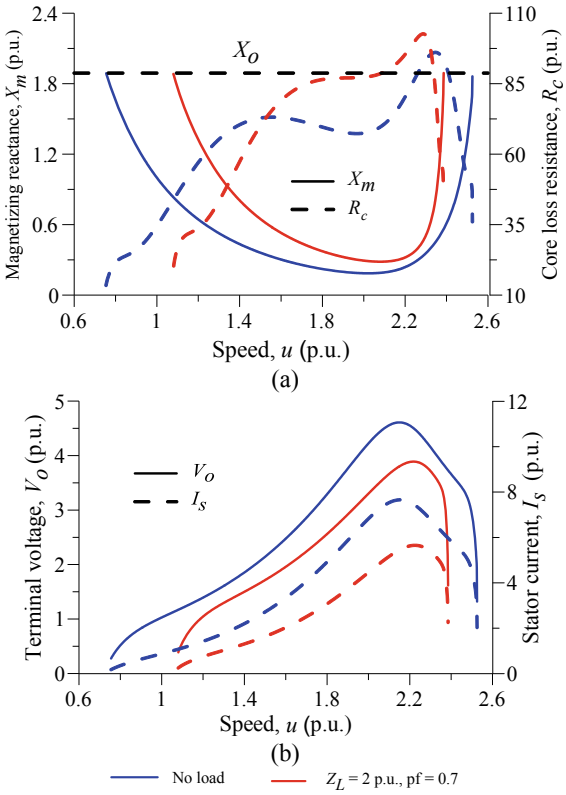

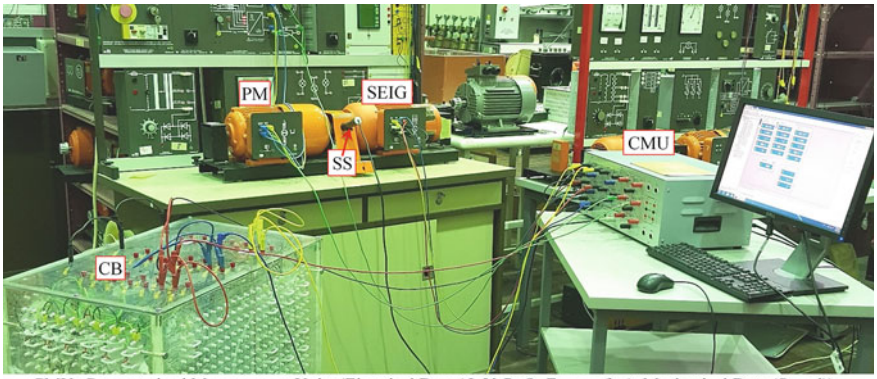

CMU: Computerized Measurement Units (Electrical Data (*I, V, P, Q, Freq., pf,…*), Mechanical Data (Speed)), SEIG: Self-Excited Induction Generator, CB: 3-phase Capacitor Bank, PM: Prime Movers, SS: Speed Sensor

Fig. 11 Experimental setup for SEIG core loss study

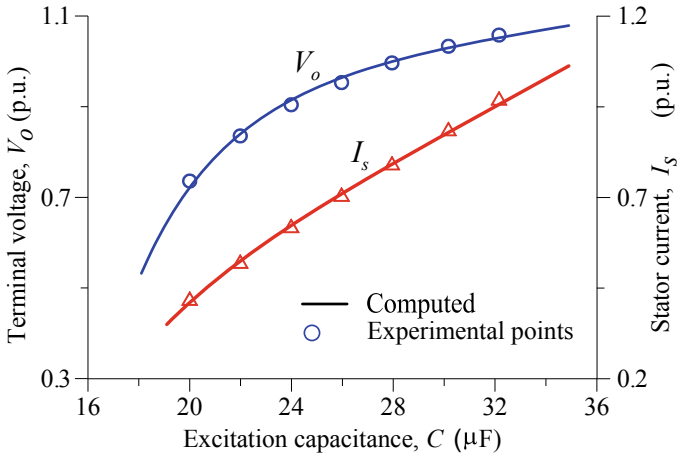

Fig. 12 Variation in stator current I_s and terminal voltage V_o against excitation capacitance C under no load ($u = 1$ p.u.)

good agreement between the simulated values and the measured results to validate the presented model.

2.3.3 Core Loss Influence

The effect of ignoring accurate modeling of core loss on the SEIG performance is discussed in this section.

The formulas that are used to evaluate the error in the values of efficiency (η) and terminal voltage (V_o) between the fixed value of R_c and the presented core loss

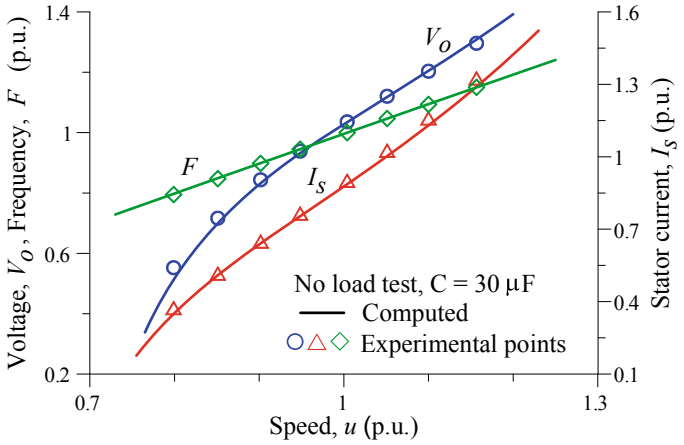

Fig. 13 Variation in stator current I_s, terminal voltage V_o, and frequency F against speed under no load

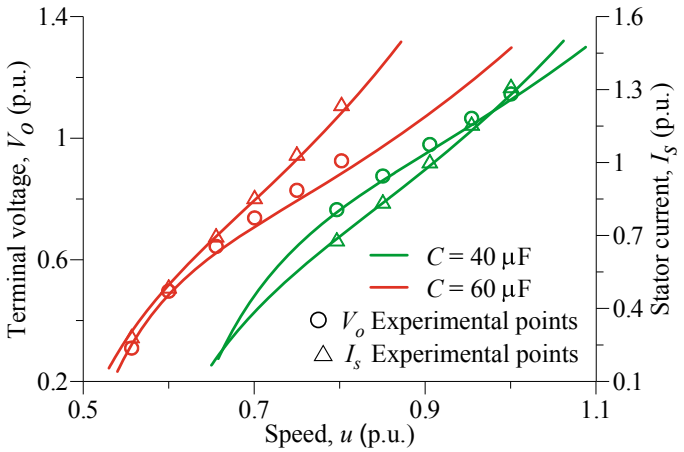

Fig. 14 Variation in stator current I_s and terminal voltage V_o against speed under no load

modeling are expressed by

$$\text{Error}(\eta) = \frac{\eta|_{R_c\text{isconstant}} - \eta|_{R_c=f(X_m)}}{\eta|_{R_c=f(X_m)}} \times 100 \tag{7}$$

$$\text{Error}(V_o) = \frac{V_o|_{R_c\text{isconstant}} - V_o|_{R_c=f(X_m)}}{V_o|_{R_c=f(X_m)}} \times 100 \tag{8}$$

Under different operating conditions, Figs. 15, 16, 17, 18, 19, 20 show the error evaluation for the system under study. The variation in the terminal voltage against

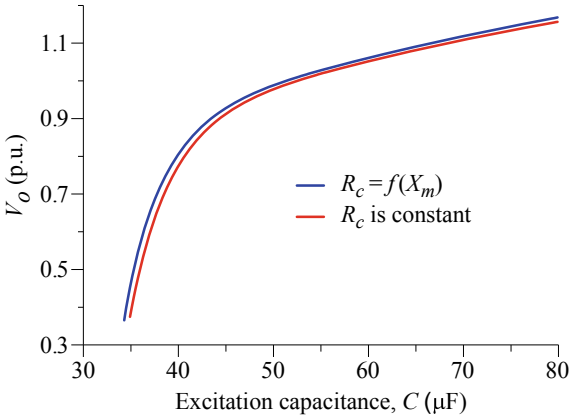

Fig. 15 Variation in terminal voltage V_o versus excitation capacitance C for two models of R_c

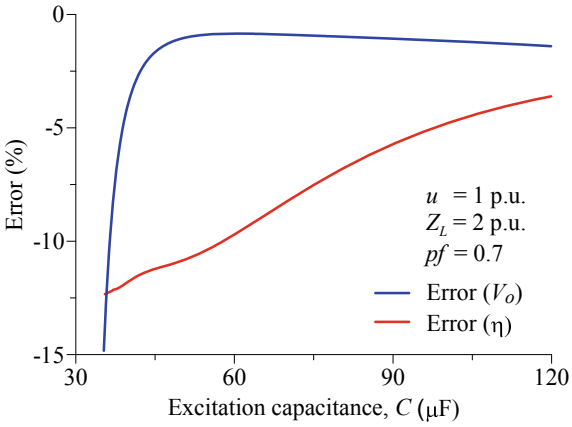

Fig. 16 Variation in the error of efficiency η and terminal voltage V_o against excitation capacitance C

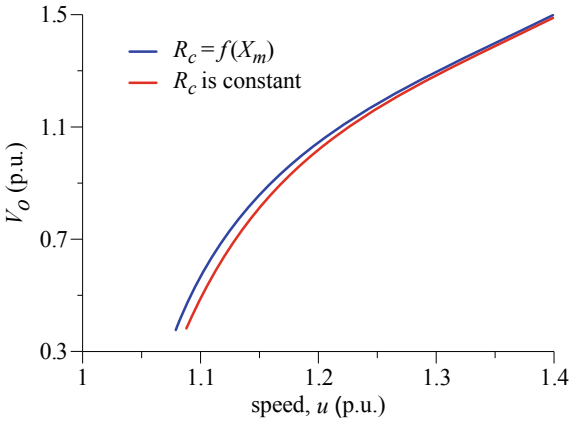

Fig. 17 Variation in terminal voltage V_o versus speed u for two models of R_c

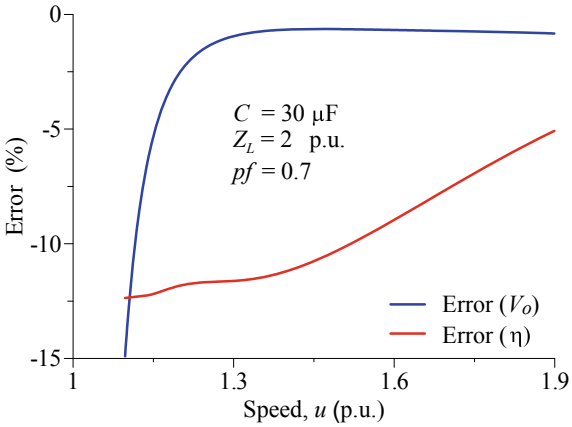

Fig. 18 Variation in the error of efficiency η and terminal voltage V_o against speed u

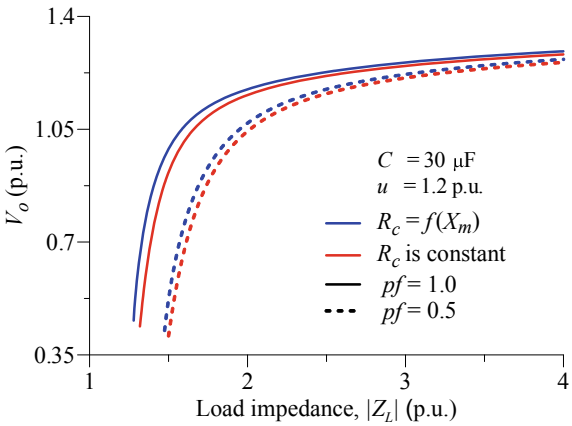

Fig. 19 Variation in the error of terminal voltage V_o against load impedance $|Z_L|$ for two models of R_c at different power factors

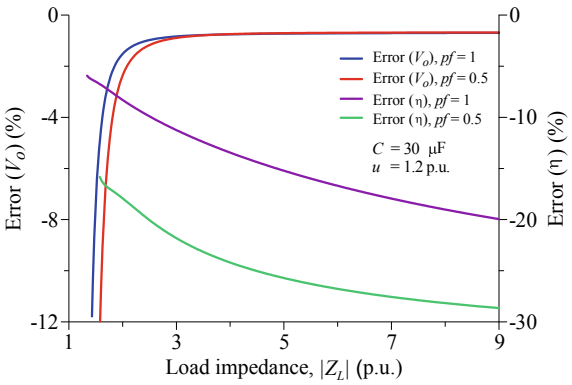

Fig. 20 Variation in error of efficiency η and terminal voltage V_o against load impedance $|Z_L|$ at different power factors

the excitation capacitor for two models of R_c is shown in Fig. 15. Figure 16 shows the error variation against excitation capacitance under fixed speed and load. The variation in the terminal voltage against the speed for the two models under fixed excitation capacitance and load is shown in Fig. 17 while the error variance of the same case is shown in Fig. 18. The conclusion from Figs. 16 and 18 is that at a low value of u and C, the error in the terminal voltage value is quite high and this error quickly decreases to an absolute low value as u, or C increase.

Figure 19 shows the variation in terminal voltage against load impedance for fixed and variable R_c under fixed excitation capacitance, power factor, and speed. Once again, at a low value of Z_L, the error in the terminal voltage value is quite high and this error rapidly decreases to an absolute low value as Z_L increases. On the other hand, the variation in the efficiency error grows up with the increase of load impedance.

3 Three-Phase Self-excited Reluctance Generator

This section presents more accurate modeling of core loss in SERG analysis taking into consideration the variation of saturation level when excitation capacitors, speed, or load change. To achieve this, the equivalent resistance of the core loss in the equivalent circuit of the generator is redeveloped, as presented below. Furthermore, a comparative study to assess the mentioned methods under different operation conditions and loads is presented. The effect of neglecting the core loss on the analysis of the SERG is discussed as well. The method presented in [35] is used as a reference to evaluate the errors in other methods.

3.1 Steady State Mathematical Model

Figure 21 shows the equivalent circuit of a three-phase self-excited reluctance generator under *R–L* load. For the performance at steady state, the following are assumed in this section to perform the analysis of the SERG [31]:

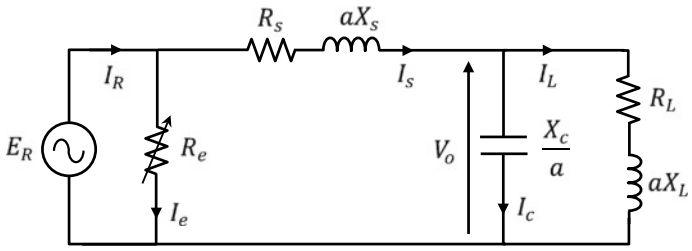

Fig. 21 Per phase equivalent circuit of the SERG

- Harmonic effects are neglected.
- The operation of the three-phase system is balanced.
- The core loss resistance R_e and the magnetizing reactance X_d are the only parameters that are affected by the saturation.
- The saturation in the quadrature axis is neglected.
- Only the reactances vary linearly with the frequency at variable speed operation.
- In the circuit of Fig. 21, all the parameters are assumed fixed and not affected by the saturation level except the magnetizing reactance X_d and the core loss resistance R_e.

The total impedance, Z_t, parallel to R_e in the circuit shown in Fig. 21 is given by

$$Z_t = R_t + jX_t = Z_s + (Z_L // Z_c) \tag{9}$$

where $Z_s = R_s + j\,a\,X_s$, $Z_L = R_L + j\,a\,X_L$, and $Z_c = -jX_c/a$.

Using d- and q-axis theory of salient pole synchronous machines, the currents and voltages are given as

$$\bar{I}_R = \bar{I}_d + \bar{I}_q \tag{10}$$

$$\bar{E}_R = -\bar{E}_q - \bar{E}_d \tag{11}$$

where $\bar{E}_q = j\,\bar{I}_d\,(aX_d)$, and $\bar{E}_d = j\,\bar{I}_q\,(aX_q)$.

In reluctance machine, the current must lead the air-gap voltage in order for it to operate as a generator. Hence, Eqs. (10) and (11) are represented as shown in Fig. 22 [30].

The current and voltage shown in Fig. 22 can be expressed as:

$$I_R^2 = I_d^2 + I_q^2 \tag{12}$$

$$E_R^2 = E_q^2 + E_d^2 = I_d^2(aX_d)^2 + I_q^2(aX_q)^2 \tag{13}$$

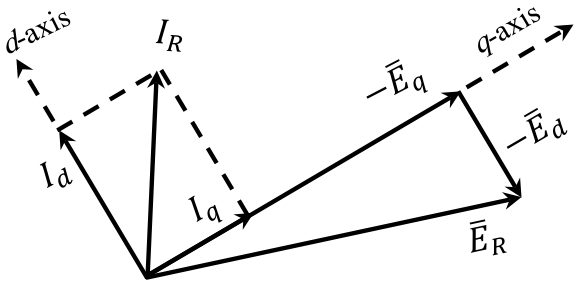

Fig. 22 Phasor diagram of the SERG